STUDY ON THE EFFECTS OF TECHNOLOGICAL PARAMETERS ON SURFACE QUALITY CHARACTERISTICS IN ULTRA-PRECISION TURNING OF DIFFRACTIVE SURFACES ON COPPER ALLOYS

NGHIÊN CỨU ẢNH HƯỞNG CỦA CÁC THÔNG SỐ CÔNG NGHỆ TỚI CÁC CHỈ TIÊU CHẤT LƯỢNG BỀ MẶT KHI TIỆN SIÊU CHÍNH XÁC BỀ MẶT NHIỄU XẠ HỢP KIM ĐỒNG

Bui Kim Hoa[1], Duong Xuan Bien[1]*, Nguyen Van Toan[1], Nguyen Kim Hung[1], Le Van Nhu[1], Pham Van Toan[2]

[1]*Le Quy Don Technical University, Ha Noi, Vietnam*
[2]*Lac Hong University, Dong Nai, Vietnam*

*Corresponding author: duongxuanbien@lqdtu.edu.vn

(Received: March 04, 2026; Revised: April 04, 2026; Accepted: May 08, 2026)

DOI: 10.31130/ud-jst.2026.24(5A).120E

Abstract - This study evaluates the independent effects of machining parameters and spindle error motion (SE) on the surface quality characteristics of copper alloy diffractive surfaces in ultra-precision turning. A novel approach is proposed by integrating SE as a covariate to quantitatively assess its influence, alongside machining parameters. The results indicate that the geometric parameters of the microstructure and the surface quality are influenced by the machining parameters. Among these, the feed rate exhibits the most significant effect on the quality indicators, followed by the spindle speed. The depth of cut has no effect on surface roughness (Sa), a slight influence on the step height (SH), and a comparable effect to spindle speed on the sidewall angle (SWA). The SE does not affect Sa and SWA, and has only a minor influence on SH.

Key words - Diffractive surface; step height (SH); sidewall angle (SWA); surface roughness (Sa); spindle error motion (SE)

Tóm tắt - Nghiên cứu này đánh giá ảnh hưởng độc lập của các thông số công nghệ gia công và sai số quay trục chính (SE) đến các đặc trưng chất lượng bề mặt mặt nhiễu xạ hợp kim đồng khi tiện siêu chính xác. Một cách tiếp cận mới được đề xuất bằng việc đưa SE vào mô hình như biến đồng phương sai để phân tích định lượng ảnh hưởng của nó cùng với các thông số công nghệ. Kết quả cho thấy các thông số hình học vi cấu trúc và chất lượng bề mặt chịu ảnh hưởng của các thông số công nghệ. Trong đó ảnh hưởng của tốc độ tiến dao tới các chỉ tiêu chất lượng là lớn nhất, sau đó là tốc độ trục chính. Chiều sâu cắt gần như không ảnh hưởng tới độ nhám (Sa), ảnh hưởng nhẹ tới chiều cao bậc (SH) và ảnh hưởng tương đương tốc độ trục chính với góc sườn (SWA). SE không ảnh hưởng đến Sa và SWA, và ảnh hưởng nhỏ tới SH.

Từ khóa - Bề mặt nhiễu xạ; chiều cao bậc; góc sườn; độ nhám bề mặt; sai số quay trục chính

1. Introduction

Ultra-precision turning (UPT) has become and continues to become one of the key machining methods in the fabrication of high-performance optical components, directly generating micro-structures by using diamond tools with small nose radius [1] and optical molds thanks to the ability of direct form generation on complex surfaces with micrometer-level form accuracy and nanometer-level surface roughness [2]. The spindle system using an aerostatic bearing provides extremely low runout during machining, thereby minimizing the errors caused by spindle error motion. An outstanding advantage of ultra-precision turning of optical surfaces is that no post-polishing is required [3], which reduces the number of processes and fabrication time while ensuring high repeatability, improving surface quality and production efficiency, and is especially suitable for the fabrication of optical elements requiring high accuracy and high surface finish as well as various types of optical molds. When optical elements are formed by mold pressing, the surface quality of the optical components after pressing is lower than that of the mold [4]. Therefore, the mold machining needs to achieve the highest possible surface quality.

In ultra-precision diamond turning, the rotational accuracy of the spindle is considered one of the factors that directly determine the form error and machined surface quality, because the error motion of the spindle changes the relative position between the tool tip and the workpiece during cutting at the nanometer level. Studies have shown that SE exists in the form of radial, axial, and tilt components, with amplitudes of only a few tens of nanometers for ultra-precision machines using aerostatic or hydrostatic bearings, but it can still cause significant form deviation on optical surfaces requiring high accuracy [5]. SE accurately reflects the actual working condition of the rotating spindle system and is commonly evaluated by the peak-to-valley (PV) value in each revolution. Zhang et al. investigated the characteristics of forced vibration caused by spindle unbalance in diamond turning and its influence on the machined surface [6]. Huang et al. [7] analyzed the effect of aerostatic SE on the surface quality of the workpiece. A method of spindle balancing by manually adding the required mass into the holes was reported by Zhang [8]. The thermal characteristics of the aerostatic bearing also affect the spindle [9].

For diffractive optical elements, the diffraction efficiency and image field quality depend not only on the overall form error but are also strongly governed by micro-geometric parameters such as the SH, SWA, and Sa of each functional zone. Many studies have shown that the deviation of SH causes direct phase error, reducing diffraction efficiency and increasing the undesired diffraction orders [10], [11], while surface roughness increases light scattering and decreases the efficiency of energy transfer into the designed diffraction order [12], [13]. At the same time, a SWA different from the ideal value will change the phase distribution and cause intensity deviation in the image plane [14]. Previous studies have indicated that the surface roughness in single-point diamond turning is strongly influenced by the feed rate, spindle speed, and tool nose radius [15]. The variation of these parameters changes the surface formation mechanism and therefore determines the level of light scattering and phase deviation of the optical element. In addition, the selection of cutting parameters and machining methods also affects burr formation, edge sharpness, and the fidelity of the micro-structure, thereby governing the actual values of SH and SWA compared to the nominal design [16].

This paper focuses on evaluating the effects of technological parameters including spindle speed, feed rate, depth of cut and SE on surface quality characteristics such as Sa, SH and SWA in ultra-precision turning of copper alloy diffractive surfaces. The results of the study not only clarify the dominant role of SE in the form accuracy of the micro-structure but also provide a scientific basis for the selection of optimal machining parameters in the fabrication of diffractive surfaces for precision optical applications.

2. Research content

2.1. Experimental setup and experimental matrix

Figure 1. *Nanoform® X ultra-precision lathe*

Figure 2. *Copper workpiece*

In this study, the ultra-precision lathe Nanoform X (Figure 1) from Precitech was used. It is widely applied in the machining of optical components, optical molds and high-precision surfaces. The machine has high stiffness, stable temperature, high vibration damping capability and high-resolution motion.

Table 1. *Chemical composition of Copper alloy*

Element	Sn	Zn	Pb	Fe	Ni	Al	Cu	Others
wt.%	0.97	40.94	2.69	0.75	0.38	0.12	54.12	0.03

The technological system of the model is described in Figure 3 with a vacuum chuck, a dedicated fixture, the workpiece, mist cooling and a diamond turning tool. The workpiece used in this study is a copper alloy (Figure 2) with the chemical composition described in Table 1. The workpiece was CNC (Computer Numerical Control) turned to generate a preliminary spherical surface profile and then mounted on the Nanoform® X for rough turning and finish turning of the diffractive surface.

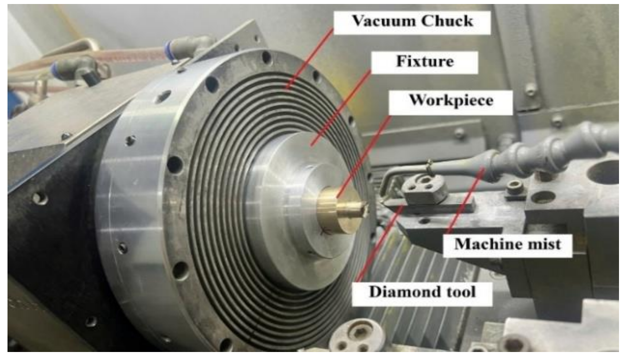

Figure 3. *Technological system of ultra-precision turning*

The single-crystal diamond turning tool (Figure 4) has the code NU160R010mWFC-MS0F20 with the tool parameters described in Table 2. Before machining, the tool was aligned with the spindle to ensure that the tool tip was located at the spindle center in order to minimize the induced error.

Figure 4. *Diamond turning tool*

Table 2. *Cutting tool parameters*

Parameter	Cutting edge radius	Rake angle	Cutting height	Included angle	First clearance
Dimensions	0.104 mm	-25°	7.405 mm	60°	12°

The input data including spindle speed n (rev/min), feed rate f (mm/min) and depth of cut ap (μm) were divided into three coded levels as shown in Table 3.

Table 3. *Values the experimental variables coding levels*

Symbol	Parameters	Levels		
		1 (-1)	2 (0)	3 (1)
x_1	n (rev/min)	1000	1500	2000
x_2	f (mm/min)	1	3	5
x_3	ap (μm)	2	5	8

From this, the experimental matrix based on the BBD model consisting of 15 experiments was established.

2.2. Diffractive surface and surface quality characteristics

The diffractive surface is composed of micro-structures including sawtooth features in order to generate the desired phase variation for the incident light wave, thereby controlling the energy distribution in the diffraction orders. The sidewall angle θ and the step height H of the diffractive surface are described as shown in Figure 5.

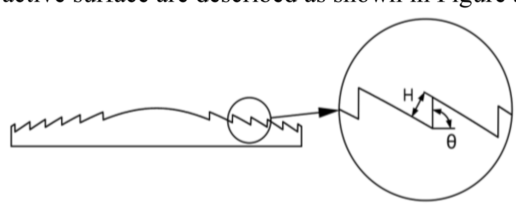

Figure 5. *Diffractive surface*

In this study, a spherical diffractive surface model was developed.

Sag equation of a spherical surface:

$$sag_{spherical} = \frac{r^2}{R\left(1+\sqrt{1-\frac{r^2}{R^2}}\right)} \quad (1)$$

Sag equation of the diffractive surface:

$$sag_{diffractive} = \frac{1}{N-1}\sum_i C_{2i} r^{2i} + \frac{\lambda}{N-1}\left[\operatorname{int}\frac{1}{\lambda}\left(\sum_i C_{2i} r^{2i}\right)\right] \quad (2)$$

The general equationcof the diffractive surface on a spherical substrate is the sum of the sag of the spherical surface and the sag of the diffractive surface:

$$sag_{total} = \frac{r^2}{R\left(1+\sqrt{1-\frac{r^2}{R^2}}\right)} + \frac{1}{N-1}\sum_i C_{2i} r^{2i} + \frac{\lambda}{N-1}\left[\operatorname{int}\frac{1}{\lambda}\left(\sum_i C_{2i} r^{2i}\right)\right] \quad (3)$$

Where: R is the vertex radius of curvature; r is the radial distance from the optical axis; λ is the wavelength of light; N is the refractive index of the lens material; C_{2i} are the diffractive coefficients.

The surface parameters are presented in Table 4.

Table 4. *Surface parameters*

Diameter	Radius of curvature	Diffractive coefficient		Wavelength	Refractive index
		C_1	C_2		
10 mm	19.5 mm	-10	-20	5000 nm	2

In UPT, the spindle is usually balanced to achieve the best machining quality. However, due to the installation of the dedicated fixture and the workpiece on the vacuum chuck, an unbalanced mass is generated. Therefore, it is necessary to readjust this unbalance before machining. The steps for checking the spindle balance are described as shown in Figure 6.

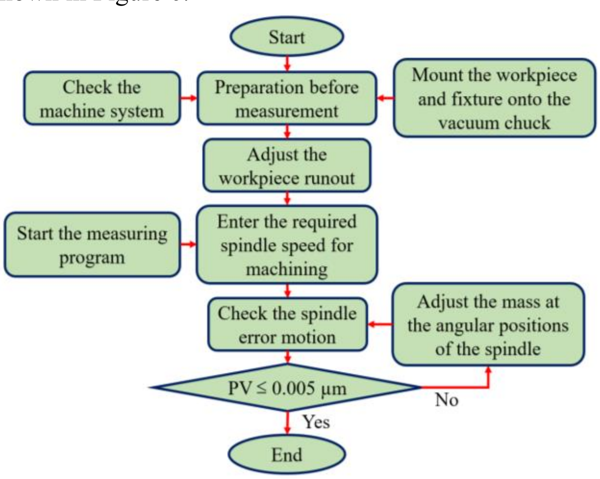

Figure 6. *Spindle balancing inspection diagram*

Step 1: Adjust the workpiece runout

Before balancing the spindle, the runout of the copper workpiece was measured using a dial indicator and adjusted to the minimum level. The position of the workpiece was corrected by gently tapping a rubber hammer on the dedicated fixture until the runout value reached the required level, in order to minimize the error caused by the setup during the balancing process.

Step 2: Enter the required spindle speed for machining

Enter the spindle speed value corresponding to the machining operation to ensure that during operation at this speed, the SE reaches the minimum value.

Step 3: Check the spindle error motion

After the spindle reaches the required speed, press "Start test" for the system to perform analysis, measurement and calculation of the spindle error motion. If the SE $PV \leq 0.005\ \mu m$ the inspection is finished. If the SE $PV > 0.005\ \mu m$ move to Step 4.

Step 4: Adjust mass at spindle angles

The display screen will indicate that additional mass needs to be added at a certain angular position of the vacuum chuck. Adjust the set screws in or out toward the spindle center by turning the threaded set screws in the threaded holes around the vacuum chuck to adjust the spindle error motion. Then return to Step 3.

The spindle can be modeled as a flexible system, where dynamic excitation caused by mass unbalance leads to radial error motion. This motion results in a deviation of the spindle center from its nominal rotational axis, thereby affecting the form accuracy and surface quality of the machined structure.

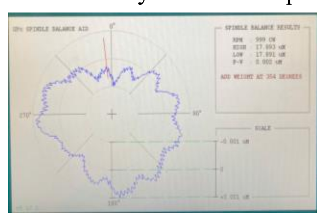

Figure 7. *Measurement results of the spindle error motion*

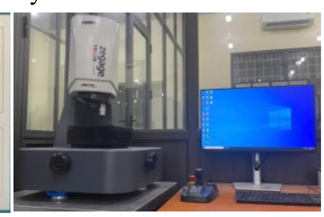

Figure 8. *Zegage Pro HR 3D Optical Measuring Machine*

Figure 7 shows the measurement results of the SE for one of the experiments.

The Sa, SWA, and SH were measured using a white light interferometer Zegage Pro HR (Figure 8). The Sa was obtained at the top of the diffractive surfaces by using the S-filter to remove system noise to obtain the primary surface, then applying Form remove to eliminate the spherical form, and finally applying the L-filter to obtain the areal surface roughness [17]. The surface roughness was measured at the crest of each diffractive structure. For each specimen, a single measurement was performed at a consistent location to ensure comparability across samples. The SWA was measured using the Inspector tool to determine the inclination of the sidewall relative to the horizontal direction after Form remove for flattening. The SWA was captured at four positions of each tooth, and at each position, measurements were performed on six random slices, with the results averaged. The SH was measured using the Mask tool to scan the areal data and take the average height difference between the two scanned regions after Form remove. SH was also measured at four captured positions on each tooth across the entire surface consisting of four diffractive teeth, resulting in a total of 16 positions over the whole surface.

2.3. Measurement results and data processing

Figure 9 and Figure 10 show the areal surface roughness measurement results. In which, Figure 9 describes the surface in the 2D view and Figure 10 describes the surface in the 3D view to clearly observe the surface undulations.

Figure 11 shows the SWA measurement result at a position of an arbitrary groove. Each slice gives a random SWA value; therefore, it is necessary to measure many slices at many positions of the grooves and take the average value to obtain the most objective result.

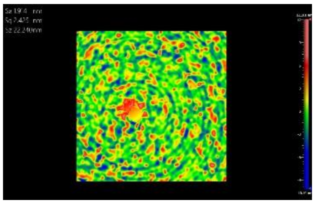

Figure 9. *2D surface roughness measurement result*

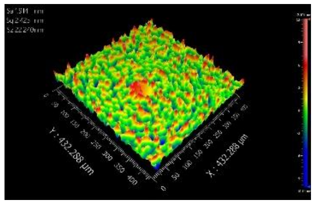

Figure 10. *3D surface roughness measurement result*

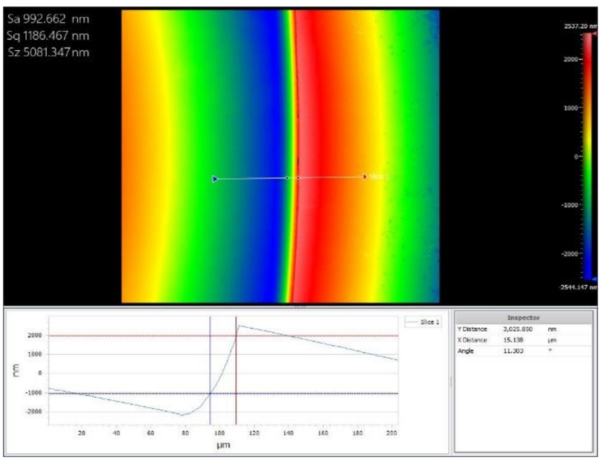

Figure 11. *Sidewall angle measurement result*

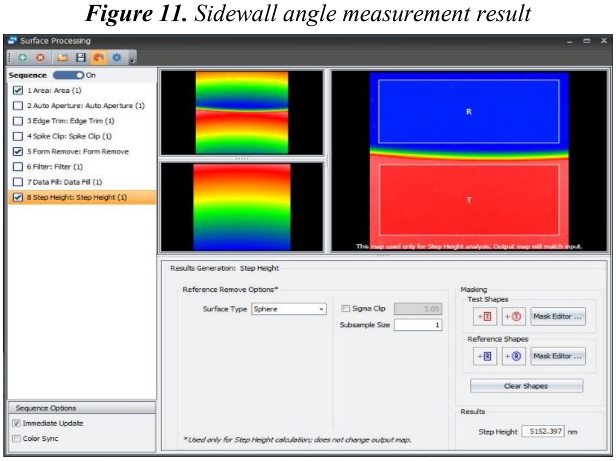

Figure 12. *Step height measurement result*

Figure 12 shows the SH measurement result after using two masks to scan the data of the Test region and the Reference region after Form remove. The measurement was carried out at many positions of the grooves and the average value was taken to obtain the most objective result.

Through the machining process and the measurement and data processing, the result table corresponding to each experiment was obtained as shown in Table 5.

From Table 6, the standard deviation (SD) of SH ranges from 110.696 to 238.061 (nm), indicating a certain level of data dispersion, though not excessive. The relative standard deviation (RSD) varies from approximately 2.145% to 4.625%, all below 5%, demonstrating good repeatability of the measurements and effective control of random errors. With the designed value of SH being 5000 nm, the absolute error (AE) and relative error (RE) are also within acceptable ranges, with RE ranging from approximately 1.586% to 3.23%, indicating that the discrepancy between the experimental and theoretical values is negligible.

Table 5. *Measurement results*

No.	n (rev/min)	f (mm/min)	ap (µm)	Sa (nm)	SWA (deg)	SH (nm)	SE (nm)
1	1000	1	5	2.601	11.705	5142.719	4
2	2000	1	5	1.874	11.862	5147.173	4
3	1000	5	5	3.958	11.634	5079.308	3
4	2000	5	5	4.304	11.122	5124.482	4
5	1000	3	2	3.364	11.678	5113.603	2
6	2000	3	2	1.682	11.672	5158.344	3
7	1000	3	8	5.157	12.007	5108.401	2
8	2000	3	8	2.383	11.958	5130.607	4
9	1500	1	2	1.914	11.445	5161.494	5
10	1500	5	2	4.179	11.505	5122.360	3
11	1500	1	8	2.925	12.321	5147.845	4
12	1500	5	8	3.905	11.390	5096.318	3
13	1500	3	5	2.269	12.317	5140.605	3
14	1500	3	5	2.366	12.343	5153.488	4
15	1500	3	5	3.432	12.385	5150.555	4

Table 6. *Statistical parameters and error analysis of SH*

No.	SH (nm)	SD	RSD (%)	AE	RE (%)
1	5142.719	202.911	3.946	142.719	2.854
2	5147.173	238.061	4.625	147.173	2.943
3	5079.308	166.289	3.274	79.308	1.586
4	5124.482	200.677	3.916	124.482	2.490
5	5113.603	138.364	2.706	113.603	2.272
6	5158.344	206.309	4.000	158.344	3.167
7	5108.401	180.413	3.532	108.401	2.168
8	5130.607	189.057	3.685	130.607	2.612
9	5161.494	110.696	2.145	161.494	3.230
10	5122.360	184.996	3.612	122.36	2.447
11	5147.845	234.476	4.555	147.845	2.957
12	5096.318	169.922	3.334	96.318	1.926
13	5140.605	206.465	4.016	140.605	2.812
14	5153.488	130.746	2.537	153.488	3.070
15	5150.555	205.162	3.983	150.555	3.011

Table 7 shows that the SD of SWA ranges from 0.09 to 0.579 (deg), indicating a certain degree of data dispersion, but still within an acceptable level. The RSD varies from approximately 0.771% to 4.822%, with most values below 5%, demonstrating good repeatability and high reliability of the measurements. With the designed value of SWA being 12.3 (deg), the AE and RE are generally low. However, in some cases, higher RE values (above 5%) are observed while RSD remains low, suggesting that these deviations may be attributed to the influence of machining parameters. Therefore, the effects of machining parameters on SWA need to be further clarified.

Table 7. *Statistical parameters and error analysis of SWA*

No.	SWA (deg)	SD	RSD (%)	AE	RE (%)
1	11.705	0.116	0.991	0.595	4.837
2	11.862	0.426	3.591	0.438	3.561
3	11.634	0.199	1.711	0.666	5.415
4	11.122	0.449	4.037	1.178	9.577
5	11.678	0.397	3.400	0.622	5.057
6	11.672	0.090	0.771	0.628	5.106
7	12.007	0.579	4.822	0.293	2.382
8	11.958	0.338	2.827	0.342	2.780
9	11.445	0.356	3.111	0.855	6.951
10	11.505	0.278	2.416	0.795	6.463
11	12.321	0.383	3.109	0.021	0.171
12	11.390	0.467	4.100	0.91	7.398
13	12.317	0.277	2.249	0.017	0.138
14	12.343	0.555	4.496	0.043	0.350
15	12.385	0.168	1.356	0.085	0.691

2.4. Investigation and discussion of the effects of technological parameters

Consider SE as a covariate factor in model development to evaluate its influence. Figure 13 shows that the input variables are independent of each other and that there is no multicollinearity among the input factors $(r = 0)$. The correlation values are $r_{SE-n} = 0.4533$ and $r_{SE-f} = -0.4533$, which indicate moderate correlations, while $r_{SE-ap} = 0$. Therefore, no serious multicollinearity is observed. Based on the variance inflation factor (VIF) values presented in Tables 7, 8, and 9, it can be observed that the three models (Sa, SWA, and SH) do not suffer from serious multicollinearity. The largest VIF value of SE is 4.49, which is still within the acceptable range, indicating that the correlation among the variables is not significant.

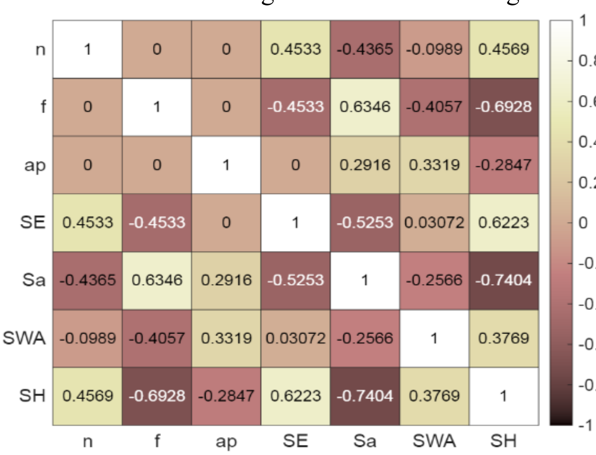

Figure 13. *Correlation coefficient*

The evaluation results of the regression models (Table 8) reveal clear differences in goodness-of-fit and predictive capability among the responses. For the Sa model, the coefficient of determination $R^2 = 0.6809$ indicates that the model explains only about 68.09% of the data variability. The $Adjusted\ R^2 = 0.5532$ and, notably, the $Predicted\ R^2 = 0.2377$ are relatively low, suggesting limited predictive capability. However, the $Adeq\ Precision = 7.1333 > 4$ indicating an adequate signal for the model, although the reliability is not high.

Table 8. *Model response indices*

	Sa	SWA	SH
R^2	0.6809	0.9938	0.9955
Adjusted R^2	0.5532	0.9782	0.9844
Predicted R^2	0.2377	0.8488	0.9122
Adeq Precision	7.1333	24.4023	32.3629

In contrast, the SWA model exhibits an excellent fit with $R^2 = 0.9938$, indicating that nearly all data variability is explained by the model. The $Adjusted\ R^2 = 0.9782$ and $Predicted\ R^2 = 0.8488$ are in reasonable agreement, confirming good predictive performance. Additionally, the $Adeq\ Precision = 24.4023$, which is much higher than the required threshold, demonstrates a very strong signal-to-noise ratio and supports the model's reliability for analysis.

Similarly, the SH model also shows a very high goodness-of-fit with $R^2 = 0.9955$, along with $Adjusted\ R^2 = 0.9844$ and $Predicted\ R^2 = 0.9122$, all of which are high and closely aligned, indicating high accuracy and excellent predictive capability. The $Adeq\ Precision = 32.3629$ further confirms a very strong signal relative to noise.

Table 9. *Analysis of variance for the regression model of Sa*

Source	Sum of Squares	Mean Square	F_{value}	p_{value}	Coef.	VIF
Model	10.45	2.61	5.33	0.0146	3.08	
A-n	1.87	1.87	3.83	0.0789	-0.5622	1.35
B-f	4.15	4.15	8.47	0.0155	0.8366	1.35
C-ap	1.30	1.30	2.66	0.1337	0.4039	1.0
D-SE	0.0412	0.0412	0.0842	0.7776	-0.1272	1.7
Residual	4.90	0.4898				
Lack of Fit	4.33	0.4811	0.8468	0.6946		
Pure Error	0.5682	0.5682				
Cor Total	15.35					

In this study, when evaluating the influence of each factor on the quality responses, the remaining factors were fixed at their center levels, and SE was set at 3.5 nm. From Table 9, it can be observed that the model is statistically significant with a $p_{value} = 0.0146 < 0.05$ and an $F_{value} = 5.33$. The lack-of-fit test is not statistically significant $p_{value} = 0.6946 > 0.05$, indicating that the model adequately fits the experimental data and can be used for prediction within the investigated range.

Based on the analysis of variance (ANOVA) results and corresponding plots (Figure 14), the feed rate is identified as the most influential factor on Sa $(p_{value} = 0.0155)$, exhibiting a positive correlation, meaning that Sa increases with increasing feed rate and vice versa. This is followed by spindle speed, which shows a marginally significant effect $(p_{value} = 0.0789)$ and a negative correlation, indicating that Sa increases as spindle speed decreases, and vice versa. For the depth of cut, although ANOVA indicates no clear statistical significance, the plots still show a slight increasing trend of Sa with increasing ap, suggesting that this factor has an effect but is not substantial. In contrast, SE has no significant effect on Sa, as evidenced by the nearly linear trend in the plot.

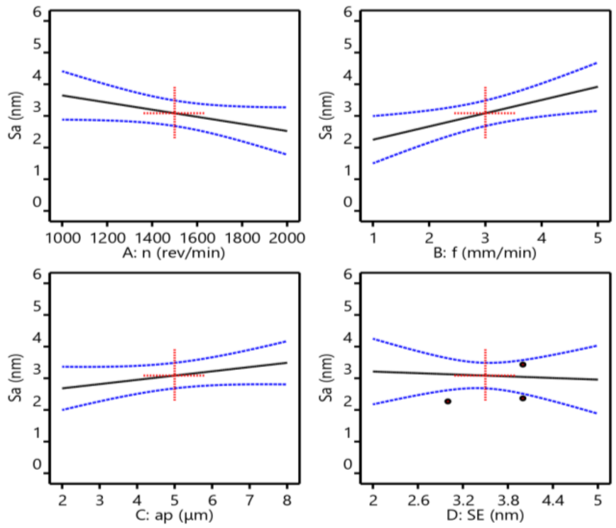

Figure 14. Effect of factors on Sa

Table 10. Analysis of variance for the regression model of SWA

Source	Sum of Squares	Mean Square	F_{value}	p_{value}	Coef.	VIF
Model	2.13	0.2135	63.74	0.0006	12.34	
A-n	0.0209	0.0209	6.23	0.0670	-0.0708	1.92
B-f	0.1512	0.1512	45.15	0.0026	-0.1907	1.92
C-ap	0.2367	0.2367	70.66	0.0011	0.1720	1.0
D-SE	0.0033	0.0033	0.9917	0.3757	0.0587	4.49
AB	0.1124	0.1124	33.56	0.0044	-0.1770	1.12
AC	0.0015	0.0015	0.4517	0.5384	-0.0205	1.12
BC	0.2379	0.2379	71.02	0.0011	-0.2575	1.12
A^2	0.2194	0.2194	65.52	0.0013	-0.2841	1.37
B^2	0.5832	0.5832	174.12	0.0002	-0.4867	1.52
C^2	0.1083	0.1083	32.34	0.0047	-0.1996	1.37
Residual	0.0134	0.0033				
Lack of Fit	0.0125	0.0042	4.73	0.3231		
Pure Error	0.0009	0.0009				
Cor Total	2.15					

The ANOVA for SWA (Table 10) indicates that the quadratic regression model is highly statistically significant, with a $p_{value} = 0.0006 < 0.05$ and a large $F_{value} = 63.74$, demonstrating that the model effectively explains the variability of the experimental data. The $Lack\ of\ fit = 0.3231 > 0.05$ is not significant, confirming that the model is adequate and can be used for prediction.

The regression equation for SWA is given as follows:

$$SWA = 12.34 - 0.1907B + 0.172C - 0.177AB \\ -0.2575BC - 0.2841A^2 - 0.4867B^2 - 0.1996C^2 \quad (4)$$

It can be observed that the influence of spindle speed on SWA is nonlinear (Figure 15). As the spindle speed increases to approximately 1500 rev/min, SWA tends to increase; however, with further increases in spindle speed, SWA decreases. The feed rate exhibits a more pronounced nonlinear effect: as the feed rate increases to about 2.5 mm/min, SWA increases, further increases in feed rate lead to a sharp decrease in SWA. For the depth of cut, SWA shows an increasing trend with increasing depth of cut, reaching a maximum at approximately 6 µm, after which further increases in depth of cut cause a slight decrease in SWA. The plot describing the effect of SE on SWA shows almost no variation, indicating that SE has no significant influence on SWA within the investigated range. Overall, the factors n, f, and ap all exhibit nonlinear effects on SWA, with the feed rate being the main dominant factor, while spindle error does not have a significant effect on SWA.

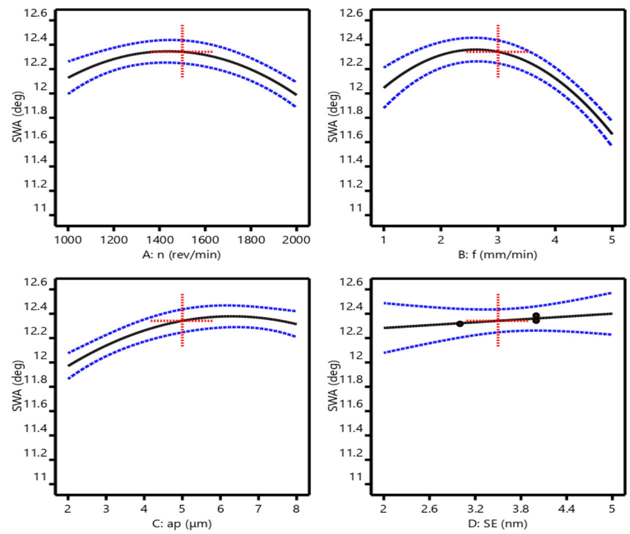

Figure 15. Effect of factors on SWA

Table 11. Analysis of variance for the regression model of SH

Source	Sum of Squares	Mean Square	F_{value}	p_{value}	Coef.	VIF
Model	8099.75	809.98	89.21	0.0003	5147.08	1.92
A-n	518.46	518.46	57.10	0.0016	11.16	1.92
B-f	1452.73	1452.73	160.01	0.0002	-18.69	1.0
C-ap	659.39	659.39	72.63	0.0010	-9.08	4.49
D-SE	100.67	100.67	11.09	0.0291	10.22	1.12
AB	257.64	257.64	28.38	0.0060	8.48	1.12
AC	193.09	193.09	21.27	0.0099	-7.34	1.12
BC	82.71	82.71	9.11	0.0392	-4.80	1.37
A^2	353.75	353.75	38.96	0.0034	-11.41	1.52
B^2	479.51	479.51	52.81	0.0019	-13.96	1.37
C^2	21.66	21.66	2.39	0.1973	-2.82	1.92
Residual	36.32	9.08				
Lack of Fit	32.02	10.67	2.48	0.4294		
Pure Error	4.30	4.30				
Cor Total	8136.07					

The ANOVA results (Table 11) indicate that the quadratic regression model developed for SH is highly statistically significant, with a $p_{value} = 0.0003 < 0.05$ and a large $F_{value} = 89.21$, demonstrating that the model effectively explains the variability of the experimental data. The $Lack\ of\ fit = 0.4294 > 0.05$ is not significant indicating that the model adequately fits the data and can be used for predictive purposes.

The regression equation for SH is given as follows:

$$SH = 5147.08 + 11.16A - 18.69B - 9.08C + 10.22D + 8.48AB - 7.34AC - 4.8BC - 11.41A^2 - 13.96B^2 \quad (5)$$

From the plots (Figure 16), SH increases as the spindle speed increases up to approximately 1800 rev/min; however, with further increases in spindle speed, SH shows a slight decreasing trend. The feed rate exhibits a decreasing effect on SH, where increasing the feed rate significantly reduces SH, particularly in the higher feed rate region, indicating that feed rate is the main dominant factor influencing SH. For the depth of cut, SH slightly decreases as the depth of cut increases, although the slope is not steep. In contrast, SE causes SH to increase, as indicated by an linear trend, although the magnitude of this effect is not large. Overall, the feed rate has the most significant influence on SH, followed by spindle speed, while the depth of cut and SE have relatively smaller effects.

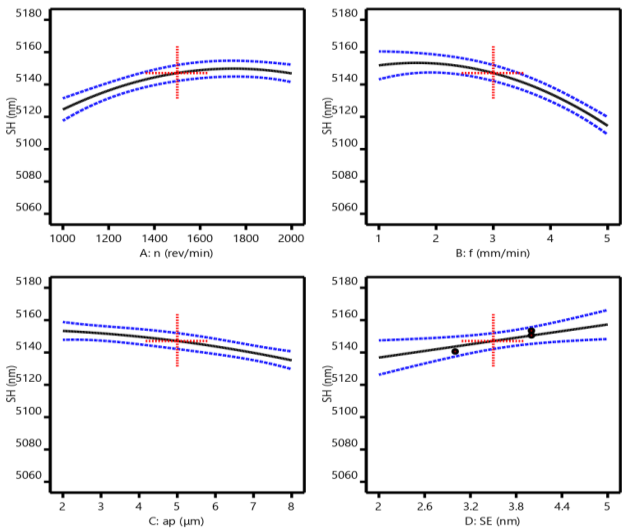

Figure 16. *Effect of factors on SH*

3. Conclusions

This study experimentally investigated the effects of individual machining parameters as well as SE on the geometric characteristics of diffractive surfaces of copper alloys during diamond turning. In general, the feed rate has the most significant influence on the surface quality indicators, followed by the spindle speed. The depth of cut has no effect on Sa, and a moderate effect on both SH and SWA. The SE has no effect on Sa and SWA, and only a slight effect on SH. Due to the limited investigation range of SE, as well as its very small magnitude at the nanometer scale, its influence on the diffractive surface quality indicators has not been fully revealed. The selection of appropriate machining parameters to achieve the desired surface quality indicators for optimal diffractive surface quality should be carefully considered. Future studies should expand the investigation range to more comprehensively evaluate the effects of machining parameters and SE on diffractive surface quality.

REFERENCES

[1] H. Liu *et al.*, "Recent advances in design and preparation of micro diamond cutting tools", *International Journal of Extreme Manufacturing*, vol. 6, Art. no. 062008, 2024. doi.org/10.1088/2631-7990/ad770d.

[2] P. Song *et al.*, "High-precision turning and ultra-smooth direct polishing of aluminum alloy mirrors", *Optics Express*, vol. 31, no. 19, pp. 30340–30358, 2023. https://doi.org/10.1364/OE.495779.

[3] S. Fujii, Y. Hayama, K. Imamura, H. Kumazaki, Y. Kakinuma, and T. Tanabe, "All-precision-machining fabrication of ultrahigh-Q crystalline optical microresonators", *Optica*, vol. 7, no. 6, pp. 694–701, 2020. https://doi.org/10.1364/OPTICA.394244.

[4] K. Li, C. Wang, and F. Gong, "The filling ratio and surface roughness evolution of glass array lens in precision glass molding", *Nanomanufacturing and Metrology*, vol. 8, Art. no. 2, 2025. doi.org/10.1007/s41871-025-00250-3.

[5] F. Ding, X. Luo, W. Chang, and Z. Wang, "In situ measurement of spindle radial and tilt error motions by complementary multi-probe method", *Nanomanufacturing and Metrology*, vol. 2, pp. 225–234, 2019. doi.org/10.1007/s41871-019-00051-5.

[6] S. J. Zhang, J. J. Yu, S. To, and Z. W. Xiong, "A theoretical and experimental study of spindle imbalance induced forced vibration and its effect on surface generation in diamond turning", *Int. J. Mach. Tools Manuf.*, vol. 133, pp. 61-71, 2018. 10.1016/j.ijmachtool s.2018.06.002.

[7] P. Huang, W. B. Lee, and C. Y. Chan, "Investigation of the effects of spindle unbalance induced error motion on machining accuracy in ultra-precision diamond turning", *International Journal of Machine Tools and Manufacture*, vol. 94, pp. 48–56, 2015. http://dx.doi.org/10.1016/j.ijmachtools.2015.04.007.

[8] L. Zhang, J. Zha, Z. Wu, and Y. Chen, "Surface finish improvement during single point diamond turning based on in-situ balancing of the spindle with CNC controller", in *Proc. 22nd Int. Conf. & Exhibition of the European Society for Precision Engineering and Nanotechnology (euspen)*, Geneva, Switzerland, May/Jun. 2022.

[9] S. Ohishi and Y. Matsuzaki, "Experimental investigation of air spindle unit thermal characteristics", *Precision Engineering*, vol 26, pp. 49–57, 2002.

[10] A. Kowalik, K. Góra, Z. Jaroszewicz, and A. Kołodziejczyk, "Multi-step electron beam technology for the fabrication of high performance diffractive optical elements", *Microelectronic Engineering*, vol. 77, pp. 347–357, 2005. doi:10.1016/j.mee.2004.1 2.036.

[11] Z. Ma, F. Kang, and H. Wang, "The impact of fabrication errors of double-layer BOE on diffraction efficiency", in *AOMATT 2016: Design, Manufacturing, and Testing of Micro- and Nano-Optical Devices and Systems; and Smart Structures and Materials*, China: Proc. SPIE, 2016, Art. no. 96850H. doi: 10.1117/12.2242497.

[12] H. Ye, J. Zhang, S. Tan, S. Zhao, M. Liu, and X. Zhang, "Analysis and prediction of effect of turning marks diffraction on image quality of optical system", *Optics and Photonics Journal*, vol. 13, pp. 97–108, 2023. https://doi.org/10.4236/opj.2023.136008.

[13] X. Zhang *et al.*, "Diffraction efficiency restoration method for a single-plane diffractive element considering machining errors", *Optics Express*, vol. 33, no. 10, pp. 21339–21353, May 2025. https://doi.org/10.1364/OE.563576.

[14] H. Vogt, R. Biertümpfel, and E. Pawlowski, "Diffractive optical elements fabricated for beam shaping of high-power diode lasers", in *High-Power Diode Laser Technology and Applications VI,* San Jose, CA, USA: Proc. SPIE, 2008, vol. 6876, Art. no. 687617. doi: 10.1117/12.763734.

[15] H. Hocheng and M. L. Hsieh, "Signal analysis of surface roughness in diamond turning of lens molds", *International Journal of Machine Tools and Manufacture*, vol. 44, pp. 1607–1618, 2004. doi:10.1016/j.ijmachtools.2004.06.003.

[16] J. Liu, S. Wang, Y. Huo, Q. Zhao, X. Wang, and J. Zhang, "An investigation of ultra-precision manufacturing methods in generating functional rectangular microstructures on the polymer material of polyimide", *Journal of Materials Research and Technology*, vol. 33, pp. 8903–8917, 2024. https://doi.org/10.1016/j.jmrt.2024.11.216.

[17] M. Raza, Z. Alam, and A. D. Udai, "ISO Standardized Form Removal and Filtering of Surface Texture for Areal Surface Roughness Measurement Using Zygo Mx," *MAPAN-Journal of Metrology Society of India,* vol 40, no. 4, pp. 937–942, 2025. https://doi.org/10.1007/s12647-025-00844-8.